Nonlin. Processes Geophys. Discuss., https://doi.org/10.5194/npg-2017-38
Manuscript under review for journal Nonlin. Processes Geophys.
Discussion started: 18 July 2017

Nonlinear Processes in Geophysics
Discussions
Open Access

Utsu aftershock productivity law explained from geometric operations on the permanent static stress field of mainshocks

Arnaud Mignan*

Institute of Geophysics, Swiss Federal Institute of Technology, Zurich

Address: ETHZ, Institute of Geophysics, NO H66, Sonneggstrasse 5, CH-8092 Zurich

Correspondence to: arnaud.mignan@sed.ethz.ch

Nonlinear Processes in Geophysics
Open Access
Discussions

Abstract: The aftershock productivity law is an exponential function of the form $K \propto \exp(\alpha M)$ with *K* the number of aftershocks, *M* the mainshock magnitude, and $\alpha \approx \ln(10)$ the productivity parameter. This law remains empirical in nature although it has also been retrieved in static stress simulations. Here, we explain this law based on Solid Seismicity, a geometrical theory of seismicity where seismicity patterns are described by mathematical expressions obtained from geometric operations on a permanent static stress field. We recover the exponential function with a break in scaling between small and large *M*, with $\alpha = 1.5\ln(10)$ and $\ln(10)$, respectively, in agreement with results from previous static stress simulations. Possible biases of aftershock selection, verified to exist in Epidemic-Type Aftershock Sequence (ETAS) simulations, may explain the lack of break in scaling observed in seismicity catalogues. The existence of the theoretical kink therefore remains to be proven.

1. Introduction

Aftershocks, the most robust patterns observed in seismicity, are characterized by three empirical laws, which are functions of time (e.g., Utsu et al., 1995; Mignan, 2015), space (e.g., Richards-Dinger et al., 2010) and mainshock magnitude (Utsu, 1970a; b; Ogata, 1988). The present study focuses on the latter relationship, i.e., the Utsu aftershock productivity law, which describes the total number of aftershocks *K* produced by a mainshock of magnitude *M* as

$$K(M) = K_0 \exp[\alpha(M - m_0)] \quad (1)$$

with m_0 the minimum magnitude cutoff (Utsu, 1970b; Ogata, 1988). This relationship was originally proposed by Utsu (1970a; b) by combining two other empirical laws, the Gutenberg-Richter relationship (Gutenberg and Richter, 1944) and Båth's law (Båth, 1964), respectively:

$$\begin{cases} N(\geq m) = A\exp[-\beta(m-m_0)] \\ N(\geq M-\Delta\mathrm{m}_B) = 1 \end{cases} \tag{2}$$

with β the magnitude size ratio (or $b = \beta/\ln(10)$ in base-10 logarithmic scale) and Δm_B the magnitude difference between the mainshock and its largest aftershock, such that

$$K(M) = N(\geq m_0|M) = \exp(-\beta\Delta\mathrm{m}_B)\exp[\beta(M-m_0)] \tag{3}$$

with $K_0 = \exp(-\beta\Delta\mathrm{m}_B)$ and $\alpha = \beta$. Eq. (3) was only implicit in Utsu (1970a) and not exploited in Utsu (1970b) where K_0 was fitted independently of the value taken by Båth's parameter Δm_B. The α-value was in turn decoupled from the β–value in later studies (e.g., Seif et al. (2017) and references therein).

Although it seems obvious that Eq. (1) can be explained geometrically if the volume of the aftershock zone is correlated to the mainshock surface area S with

$$S(M) = 10^{M-4} = \exp[\ln(10)(M-4)] \tag{4}$$

(Kanamori and Anderson, 1975; Yamanaka and Shimazaki, 1990; Helmstetter, 2003), there is so far no analytical, physical expression of Eq. (1) available. Although Hainzl et al. (2010) retrieved the exponential behavior in numerical simulations where aftershocks were produced by the permanent static stress field of mainshocks of different magnitudes, it remains unclear how K_0 and α relate to the underlying physical parameters.

The aim of the present article is to explain the Utsu aftershock productivity equation (Eq. 1) by applying a geometrical theory of seismicity (or "Solid Seismicity"), which has already been shown to effectively explain other empirical laws of both natural and induced seismicity from simple geometric operations on a permanent static stress field (Mignan, 2012; 2016a). The theory is applied here for the first time to the case of aftershocks.

Nonlin. Processes Geophys. Discuss., https://doi.org/10.5194/npg-2017-38
Manuscript under review for journal Nonlin. Processes Geophys.
Discussion started: 18 July 2017

2. Physical Expression of Aftershock Productivity

"Solid Seismicity", a geometrical theory of seismicity, is based on the following Postulate (Mignan et al., 2007; Mignan, 2008, 2012; 2016a):

Solid Seismicity Postulate (SSP): *Seismicity can be strictly categorized into three regimes of constant spatiotemporal densities – background δ_0, quiescence δ_- and activation δ_+ (with $\delta_- \ll \delta_0 \ll \delta_+$) - occurring respective to the static stress step function:*

$$\delta(\sigma) = \begin{cases} \delta_- & , \sigma < -\Delta o_* \\ \delta_0 & , \sigma \leq |\pm\Delta o_*| \\ \delta_+ & , \sigma > \Delta o_* \end{cases} \quad (5)$$

with Δo_* the background stress amplitude range.

Based on this Postulate, Mignan (2012) demonstrated the power-law behavior of precursory seismicity in agreement with the observed time-to-failure equation (Varnes, 1989), while Mignan (2016a) demonstrated both the observed parabolic spatiotemporal front and the linear relationship with injection-flow-rate of induced seismicity (Shapiro and Dinske, 2009). It remains unclear whether the SSP has a physical origin or not. If not, it would still represent a reasonable approximation of the linear relationship between event production and static stress field in a simple clock-change model (Hainzl et al., 2010) (Fig. 1a). The power of Eq. (5) is that it allows defining seismicity patterns in terms of "solids" described by the spatial envelope $r_* = r(\sigma = \pm\Delta o_*)$. The spatiotemporal rate of seismicity is then a mathematical expression defined by the density of events δ times the volume characterized by r_* (see previous demonstrations in Mignan et al. (2007) and Mignan (2011; 2012; 2016a) where simple algebraic expressions were obtained).

In the case of aftershocks, we define the static stress field of the mainshock by

$$\sigma(r) = -\Delta\sigma_0 \left[\left(1 - \frac{c^3}{(r+c)^3}\right)^{-1/2} - 1 \right] \quad (6)$$

with $\Delta\sigma_0 < 0$ the mainshock stress drop, c the crack radius and r the distance from the crack. Eq (6) is a simplified representation of stress change from slip on a planar surface in a homogeneous elastic medium. It takes into account both the square root singularity at crack tip and the $1/r^3$ falloff at higher distances (Dieterich, 1994) (Fig. 1b). It should be noted that this radial static stress field does not represent the geometric complexity of Coulomb stress fields (Fig. 2a). However we are here only interested in the general behavior of aftershocks with Eq. (6) retaining the first-order characteristics of this field (i.e., on-fault seismicity; Fig. 2b), which corresponds to the case where the mainshock relieves most of the regional stresses and aftershocks occur on optimally oriented faults. It is also in agreement with observations, most aftershocks being located on and around the mainshock fault traces in Southern California (Fig. 2c; see section "Observations & Model Fitting"). The occasional cases where aftershocks occur off-fault (e.g., Ross et al., 2017) can be explained by the mainshock not relieving all of the regional stress (King et al., 1994) (Fig. 2d).

For $r_* = r(\sigma = \Delta o_*)$, Eq. (6) yields the aftershock solid envelope of the form:

$$r_*(c) = \left\{ \frac{1}{\left[1 - \left(1 - \frac{\Delta\sigma_*}{\Delta\sigma_0}\right)^{-2}\right]^{1/3}} - 1 \right\} c = Fc \quad (7)$$

, function of the crack radius c and of the ratio between background stress amplitude range Δo_* and stress drop $\Delta\sigma_0$ (Fig. 1c). With $\Delta\sigma_0$ independent of earthquake size (Kanamori and Anderson, 1975; Abercrombie and Leary, 1993) and Δo_* assumed constant, r_* is directly proportional to c with proportionality constant, or stress factor, F (Eq. 7). Geometrical constraints due to the seismogenic layer width w_0 then yield

Nonlin. Processes Geophys. Discuss., https://doi.org/10.5194/npg-2017-38
Manuscript under review for journal Nonlin. Processes Geophys.
Discussion started: 18 July 2017

Nonlinear Processes in Geophysics
Discussions
Open Access

$$c(M) = \begin{cases} \left(\frac{S(M)}{\pi}\right)^{1/2} & , S(M) \leq \pi w_0^2 \\ w_0 & , S(M) > \pi w_0^2 \end{cases} \tag{8}$$

with S the rupture surface defined by Eq. (4) and c becoming an effective crack radius (Kanamori and Anderson, 1975) (Fig. 1d). Note that the factor of 2 (i.e., using w_0 instead of $w_0/2$) comes from the free surface effect (e.g., Kanamori and Anderson, 1975; Shaw and Scholz, 2001).

The aftershock productivity $K(M)$ is then the activation density δ_+ times the volume $V_*(M)$ of the aftershock solid. For the case in which the mainshock relieves most of the regional stress, stresses are increased all around the rupture (King et al., 1994), which is topologically identical to stresses increasing radially from the rupture plane (Fig. 2a-b). It follows that the aftershock solid can be represented by a volume of contour $r_*(M)$ from the rupture plane geometric primitive, i.e., a disk or a rectangle, for small and large mainshocks respectively. This is illustrated in Figure 3a-b and can be generalized by

$$V_*(M) = 2r_*(M)S(M) + \frac{\pi}{2}r_*^2(M)d \tag{9}$$

where d is the distance travelled around the geometric primitive by the geometric centroid of the semi-circle of radius $r_*(M)$ (i.e., Pappus's Centroid Theorem), or

$$d = \begin{cases} 2\pi\left(c(M) + \frac{4}{3\pi}r_*(M)\right) & , c(M) + r_*(M) \leq \frac{w_0}{2} \\ 2w_0 & , c(M) + r_*(M) > \frac{w_0}{2} \end{cases} \tag{10}$$

For the disk, the volume (Eq. 9) corresponds to the sum of a cylinder of radius $c(M)$ and height $2r_*(M)$ (first term) and of half a torus of major radius $c(M)$ and minus radius $r_*(M)$ (second term). For the rectangle, the volume is the sum of a cuboid of length $l(M)$ (i.e., rupture length), width w_0 and height $2r_*(M)$ (first term) and of a cylinder of radius $r_*(M)$ and height w_0 (second term; see red and orange volumes,

Nonlin. Processes Geophys. Discuss., https://doi.org/10.5194/npg-2017-38
Manuscript under review for journal Nonlin. Processes Geophys.
Discussion started: 18 July 2017

Nonlinear Processes in Geophysics Open Access Discussions

respectively, in Figure 3a-c). Finally inserting Eqs. (7), (8) and (10) into (9), we obtain

$$K(M) = \delta_+(m_0) \begin{cases} \left[\frac{2F}{\sqrt{\pi}} + F^2\sqrt{\pi}\left(1 + \frac{4}{3\pi}F\right)\right] S^{3/2}(M) & , S(M) \le \left(\frac{w_0\sqrt{\pi}}{2(1+F)}\right)^2 \\ \frac{2F}{\sqrt{\pi}} S^{3/2}(M) + F^2 w_0 S(M) & \left(\frac{w_0\sqrt{\pi}}{2(1+F)}\right)^2 < S(M) \le \pi w_0^2 \\ 2F w_0 S(M) + \pi F^2 w_0^3 & , S(M) > \pi w_0^2 \end{cases}$$

(11)

which is represented in Figure 3d. Considering the two main regimes only (small versus large mainshocks) and inserting Eq. (4) into (11), we get

$$K(M) = \delta_+(m_0) \begin{cases} \left[\frac{2F}{\sqrt{\pi}} + F^2\sqrt{\pi}\left(1 + \frac{4}{3\pi}F\right)\right] \exp\left[\frac{3\ln(10)}{2}(M-4)\right] & , \text{small } M \\ 2F w_0 \exp[\ln(10)(M-4)] + \pi F^2 w_0^3 & , \text{large } M \end{cases}$$

(12)

which is a closed-form expression of the same form as the original Utsu productivity law (Eq. 1).

Here, we predict that the α-value decreases from 3ln(10)/2 ≈ 3.45 to ln(10) ≈ 2.30 when switching regime from small to large mainshocks (or from 1.5 to 1 in base-10 logarithmic scale). It should be noted that Hainzl et al. (2010) observed the same break in scaling in static stress transfer simulations, which corroborates our analytical findings. For large *M*, the scaling is fundamentally the same as in Eq. (4). Since that relation also explains the slope of the Gutenberg-Richter law (see physical explanation given by Kanamori and Anderson (1975)), it follows that $\alpha \equiv \beta$, which is also in agreement with the original formulation of Utsu (1970a; b) (Eq. 3).

3. Observations & Model Fitting

We consider the case of Southern California and extract aftershock sequences from the relocated earthquake catalog of Hauksson et al. (2012) defined over the

Nonlin. Processes Geophys. Discuss., https://doi.org/10.5194/npg-2017-38
Manuscript under review for journal Nonlin. Processes Geophys.
Discussion started: 18 July 2017

Nonlinear Processes in Geophysics
Discussions

period 1981-2011, using the nearest-neighbor method (Zaliapin et al., 2008) (used with its standard parameters originally calibrated for Southern California). Only events with magnitudes greater than $m_0 = 2.0$ are considered (a conservative estimate following results of Tormann et al. (2014); saturation effects immediately after the mainshock are negligible when considering entire aftershock sequences; Helmstetter et al. (2005)). The observed number of aftershocks n produced by a mainshock of magnitude M (for a total of N mainshocks) is shown in Figure 4a.

We first fit Eq. (1) to the data using the Maximum Likelihood Estimation (MLE) method with the log-likelihood function

$$LL(\theta; X = \{n_i; i = 1, \ldots, N\}) = \sum_{i=1}^{N} [n_i \ln[K_i(\theta)] - K_i(\theta) - \ln(n_i!)] \qquad (13)$$

for a Poisson process, or, with Eq. (1),

$$LL(\theta = \{K_0, \alpha\}; X) = \ln(K_0) \sum_{i=1}^{N} n_i + \alpha \sum_{i=1}^{N} [n_i (M_i - m_0)] - K_0 \sum_{i=1}^{N} \exp[\alpha(M_i - m_0)] - \sum_{i=1}^{N} \ln(n_i!) \qquad (14)$$

(note that the last term can be set to 0 during LL maximization). For Southern California, we obtain $\alpha_{\mathrm{MLE}} = 2.04$ (0.89 in $\log_{10}$ scale) and $K_0 = 0.23$. It should be noted that this approach does not include the case of mainshocks that produce zero aftershock. Therefore we also compute the MLE for the Zero-Inflated Poisson (ZIP) distribution:

$$\begin{cases} \Pr(n_i = 0) = w + (1 - w)\exp(-K_i) \\ \Pr(n_i > 0) = (1 - w)\frac{{K_i}^{n_i}}{n_i!}\exp(-K_i) \end{cases} \qquad (15)$$

where w is a weighting constant. It finally follows that $\alpha_{\mathrm{MLE(ZIP)}} = 2.13$ (0.93 in $\log_{10}$ scale, with $K_0 = 0.15$), corrected for zero-values. This result is in agreement with previous studies in the same region (e.g., Helmstetter, 2003; Helmstetter et al., 2005; Zaliapin and Ben-Zion, 2013; Seif et al., 2017) and with $\alpha = \ln(10) \approx 2.30$ predicted for large mainshocks in Solid Seismicity. Moreover we find a bulk $\beta_{\mathrm{MLE}} = 2.34$ (1.02

Nonlin. Processes Geophys. Discuss., https://doi.org/10.5194/npg-2017-38
Manuscript under review for journal Nonlin. Processes Geophys.
Discussion started: 18 July 2017

in $\log_{10}$ scale) (Aki, 1965), in agreement with $\alpha = \beta$. It should be noted that no significant difference is obtained when computing β_{MLE} for background events or aftershocks alone, with $\beta_{MLE} = 2.29$ and 2.35, respectively (0.99 and 1.02 in $\log_{10}$ scale).

We also tested the following piecewise model to identify any break in scaling, as predicted by Eq. (12):

$$K(M) = \begin{cases} K_0 \frac{\exp[\ln(10)(M_{break}-m_0)]}{\exp\left[\frac{3}{2}\ln(10)(M_{break}-m_0)\right]} \exp\left[\frac{3}{2}\ln(10)(M-m_0)\right] & , M \leq M_{break} \\ K_0 \exp[\ln(10)(M-m_0)] & , M > M_{break} \end{cases}$$

(16)

but with the best MLE result obtained for $M_{break} = m_0$, suggesting no break in scaling in the aftershock productivity data.

4. Role of aftershock selection on productivity scaling-break

We now identify whether the lack of break in scaling in aftershock productivity observed in earthquake catalogues could be an artefact related to the aftershock selection method. We run Epidemic-Type Aftershock Sequence (ETAS) simulations (Ogata, 1988; Ogata and Zhuang, 2006), with the seismicity rate

$$\begin{cases} \lambda(t,x,y) = \mu(t,x,y) + \sum_{i:t_j<t} K(M_i) f(t-t_i) g(x-x_i, y-y_i | M_i) \\ f(t) = c^{p-1}(p-1)(t+c)^{-p} \\ g(x,y|M) = \frac{1}{\pi}\left(de^{\gamma(M-m_0)}\right)^{q-1}\left(x^2+y^2+de^{\gamma(M-m_0)}\right)^{-q}(q-1) \end{cases} \quad (17)$$

Aftershock sequences are defined by power laws, both in time and space (for an alternative temporal function, see Mignan (2015; 2016b)). μ is the Southern California background seismicity, as defined by the nearest-neighbor method (with same t, x, y and m). We fix the ETAS parameters to $\theta = \{c = 0.011$ day, $p = 1.08$, $d = 0.0019$ km^2, $q = 1.47$, $\gamma = 2.01\}$, following the fitting results of Seif et al. (2017) for the Southern California relocated catalog and $m_0 = 2$ (see their Table 1). However, we define the productivity $K(M)$ from Eq. (16) with $M_{break} = 5$, $K_0 = 0.23$, $\alpha = 2.04$ and $\beta = 2.3$. Examples of ETAS simulations are shown in Figure 4b for comparison with the observed Southern California time series. Figure 4c allows us to verify that the simulated aftershock productivity is kinked at M_{break}, as defined by Eq. (16).

We then select aftershocks from the ETAS simulations with the nearest-neighbor method. Figure 4d represents the estimated aftershock productivity, which has lost the break in scaling originally implemented in the simulations. Note that a similar result is obtained when using a windowing method (Gardner and Knopoff, 1974). This demonstrates that the theoretical break in scaling predicted in the aftershock productivity law can be lost in observations due to an aftershock selection bias, all declustering techniques assuming continuity over the entire magnitude range. While such a bias is possible, it yet does not prove that the break in scaling exists. The fact that a similar break in scaling was obtained in independent Coulomb stress simulations (Hainzl et al., 2010) however provides high confidence in our results.

5. Conclusions

In the present study, a physical closed-form expression defined from geometric and static stress parameters was proposed (Eq. 12) to explain the empirical Utsu aftershock productivity law (Eq. 1). This demonstration, combined to the previous ones made by the author to explain precursory accelerating seismicity and induced seismicity (Mignan, 2012; 2016b), suggests that most empirical laws observed in seismicity populations can be explained by simple geometric operations on a permanent static stress field. Although the Solid Seismicity Postulate (SSP) (Eq. 5) remains to be proven, it is so far a rather convenient and pragmatic assumption to determine the physical parameters that play a first-order role in the behavior of seismicity. It is also complementary to the more common simulations of static stress loading (King and Bowman, 2003) and static stress triggering (Hainzl et al., 2010). Analytic geometry, providing both a visual representation and an analytical expression of the problem at hand (Fig. 3), represents a new approach to try better understanding the behavior of seismicity. Its current limitation in the case of aftershock analysis consists in assuming that the static stress field is radial and described by Eq. (6) (Dieterich, 1994), which is likely only valid for mainshocks relieving most of the regional stresses and with aftershocks occurring on optimally oriented faults (King et al., 1994). More complex, second-order, stress behaviors might explain part of the scattering observed around Eq. (1) (Fig. 4a). Other $\sigma(r)$ formulations could be tested in the future, the only constraint on generating so-called seismicity solids being the use of the postulated static stress step function of Eq. (5) (i.e., the Solid Seismicity Postulate, SSP).

References

Abercrombie, R. and Leary, P.: Source parameters of small earthquakes recorded at 2.5 km depth, Cajon Pass, Southern California: Implications for earthquake scaling, Geophys. Res. Lett., 20, 1511-1514, 1993.

Aki, K.: Maximum Likelihood Estimate of b in the Formula log N = a-bM and its Confidence Limits, Bull. Earthq. Res. Instit., 43, 237-239, 1965.

Båth, M.: Lateral inhomogeneities of the upper mantle, Tectonophysics, 2, 483-514, 1965.

Dieterich, J.: A constitutive law for rate of earthquake production and its application to earthquake clustering, J. Geophys. Res., 99, 2601-2618, 1994.

Gardner, J. K. and Knopoff, L.: Is the sequence of earthquakes in Southern California, with aftershocks removed, Poissonian?, Bull. Seismol. Soc. Am., 64, 1363-1367, 1974.

Gutenberg, B. and Richter, C. F.: Frequency of earthquakes in California, Bull. Seismol. Soc. Am., 34, 185-188, 1944.

Hainzl, S., Brietzke, G. B. and Zöller, G.: Quantitative earthquake forecasts resulting from static stress triggering, J. Geophys. Res., 115, B11311, doi: 10.1029/2010JB007473, 2010.

Hauksson, E., Yang, W. and Shearer, P. M.: Waveform Relocated Earthquake Catalog for Southern California (1981 to June 2011), Bull. Seismol. Soc. Am., 102, 2239-2244, doi: 10.1785/0120120010, 2012.

Helmstetter, A.: Is Earthquake Triggering Driven by Small Earthquakes?, Phys. Rev. Lett., 91, doi: 10.1102/PhysRevLett.91.058501, 2003.

Helmstetter, A., Kagan, Y. Y. and Jackson, D. D. : Importance of small earthquakes for stress transfers and earthquake triggering, J. Geophys. Res., 110, B05S08, doi: 10.1029/2004JB003286, 2005.

Kanamori, H. and Anderson, D. L.: Theoretical basis of some empirical relations in seismology, Bull. Seismol. Soc. Am., 65, 1073-1095, 1975.

King, G. C. P., Stein, R. S. and Lin, J.: Static Stress Changes and the Triggering of Earthquakes, Bull. Seismol. Soc. Am., 84, 935-953, 1994.

King, G. C. P. and Bowman, D. D.: The evolution of regional seismicity between large earthquakes, J. Geophys. Res., 108, 2096, doi: 10.1029/2001JB000783, 2003.

Lin, J. and Stein, R. S.: Stress triggering in thrust and subduction earthquakes, and stress interaction between the southern San Andreas and nearby thrust and strike-slip faults, J. Geophys. Res., 109, B02303, doi: 10.1029/2003JB002607, 2004.

Nonlin. Processes Geophys. Discuss., https://doi.org/10.5194/npg-2017-38
Manuscript under review for journal Nonlin. Processes Geophys.
Discussion started: 18 July 2017

Nonlinear Processes in Geophysics
Discussions
Open Access

Mignan, A., King, G. C. P. and Bowman, D.: A mathematical formulation of accelerating moment release based on the stress accumulation model, J. Geophys. Res., 112, B07308, doi: 10.1029/2006JB004671, 2007.

Mignan, A.: Non-Critical Precursory Accelerating Seismicity Theory (NC PAST) and limits of the power-law fit methodology, Tectonophysics, 452, 42-50, doi: 10.1016/j.tecto.2008.02.010, 2008.

Mignan, A.: Retrospective on the Accelerating Seismic Release (ASR) hypothesis: Controversy and new horizons, Tectonophysics, 505, 1-16, doi: 10.1016/j.tecto.2011.03.010, 2011.

Mignan, A.: Seismicity precursors to large earthquakes unified in a stress accumulation framework, Geophys. Res. Lett., 39, L21308, doi: 10.1029/2012GL053946, 2012.

Mignan, A.: Modeling aftershocks as a stretched exponential relaxation, Geophys. Res. Lett., 42, 9726-9732, doi: 10.1002/2015GL066232, 2015.

Mignan, A.: Static behaviour of induced seismicity, Nonlin. Processes Geophys., 23, 107-113, doi: 10.5194/npg-23-107-2016, 2016a.

Mignan, A.: Reply to "Comment on 'Revisiting the 1894 Omori Aftershock Dataset with the Stretched Exponential Function' by A. Mignan" by S. Hainzl and A. Christophersen, Seismol. Res. Lett., 87, 1134-1137, doi: 10.1785/0220160110, 2016b.

Ogata, Y.: Statistical Models for Earthquake Occurrences and Residual Analysis for Point Processes, J. Am. Stat. Assoc., 83, 9-27, 1988.

Ogata, Y. and Zhuang, J.: Space-time ETAS models and an improved extension, Tectonophysics, 413, 13-23, doi: 10.1016/j.tecto.2005.10.016, 2006.

Richards-Dinger, K., Stein, R. S. and Toda, S.: Decay of aftershock density with distance does not indicate triggering by dynamic stress, Nature, 467, 583-586, doi: 10.1038/nature09402, 2010.

Ross, Z. E., Hauksson, E. and Ben-Zion, Y.: Abundant off-fault seismicity and orthogonal structures in the San Jacinto fault zone, Sci. Adv., 3, doi: 10.1126/sciadv.1601946, 2017.

Seif, S., Mignan, A., Zechar, J. D., Werner, M. J. and Wiemer, S.: Estimating ETAS: The effects of truncation, missing data, and model assumptions, J. Geophys. Res. Solid Earth, 121, 449-469, doi: 10.1002/2016JB012809, 2017.

Shapiro, S. A. and Dinske, C.: Scaling of seismicity induced by nonlinear fluid-rock interaction, J. Geophys. Res., 114, B09307, doi: 10.1029/2008JB006145, 2009.

Shaw, B. E. and Scholz, C. H.: Slip-length scaling in large earthquakes: Observations and theory and implications for earthquake physics, Geophys. Res. Lett., 28, 2995-2998, 2001.

Toda, S., Stein, R. S., Richards-Dinger, K. and Bozkurt, S.: Forecasting the evolution of seismicity in southern California: Animations built on earthquake stress transfer, J. Geophys. Res., 110, B05S16, doi: 10.1029/2004JB003415, 2005.

Tormann, T., Wiemer, S. and Mignan, A.: Systematic survey of high-resolution b value imaging along Californian faults: inference on asperities, J. Geophys. Res. Solid Earth, 119, 2029-2054, doi: 10.1002/2013JB010867, 2014.

Utsu, T.: Aftershocks and Earthquake Statistics (1): Some Parameters Which Characterize an Aftershock Sequence and Their Interrelations, J. Faculty Sci. Hokkaido Univ. Series 7 Geophysics, 3, 129-195, 1970a.

Utsu, T.: Aftershocks and Earthquake Statistics (2): Further Investigation of Aftershocks and Other Earthquake Sequences Based on a New Classification of

Earthquake Sequences, J. Faculty Sci. Hokkaido Univ. Series 7 Geophysics, 3, 197-266, 1970b.

Utsu, T., Ogata,, Y. and Matsu'ura, R. S.: The Centenary of the Omori Formula for a Decay Law of Aftershock Activity, J. Phys. Earth, 43, 1-33, 1995.

Varnes, D. J.: Predicting Earthquakes by Analyzing Accelerating Precursory Seismic Activity, Pure Appl. Geophys., 130, 661-686, 1989.

Yamanaka, Y. and Shimazaki, K.: Scaling Relationship between the Number of Aftershocks and the Size of the Main Shock, J. Phys. Earth, 38, 305-324, 1990.

Zaliapin, I., Gabrielov, A., Keilis-Borok, V. and Wong, H.: Clustering Analysis of Seismicity and Aftershock Identification, Phys. Rev. Lett., 101, 018501, doi: 10.1103/PhysRevLett.101.018501, 2008.

Zaliapin, I. and Ben-Zion, Y.: Earthquake clusters in southern California I: Identification and stability, J. Geophys. Res. Solid Earth, 118, 2847-2864, doi: 10.1002/jgrb.50179, 2013.

Figures

Nonlin. Processes Geophys. Discuss., https://doi.org/10.5194/npg-2017-38
Manuscript under review for journal Nonlin. Processes Geophys.
Discussion started: 18 July 2017

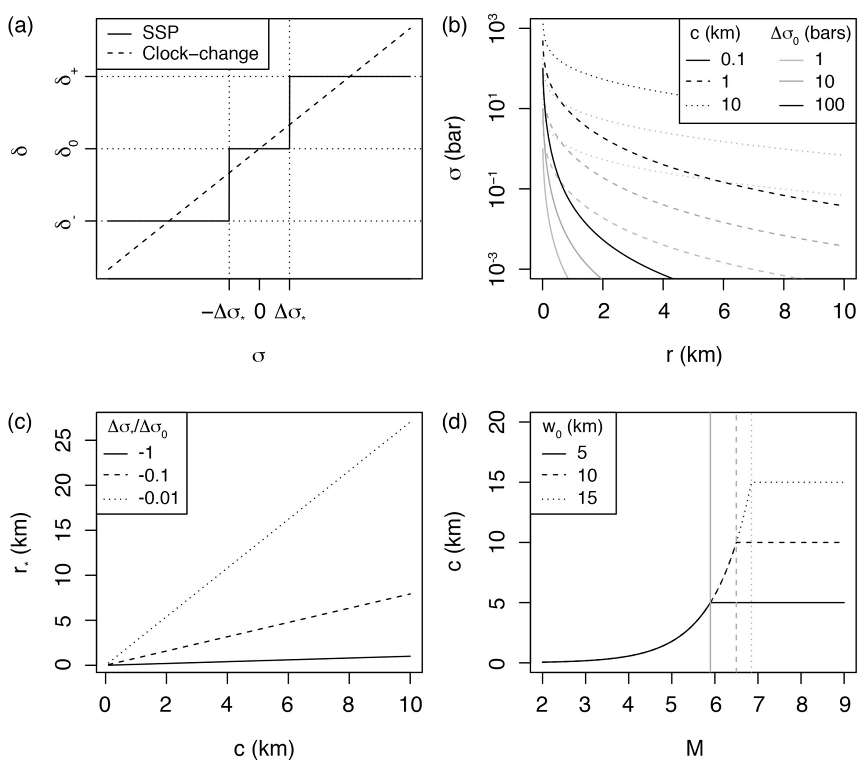

Figure 1. Definition of the aftershock solid envelope in a permanent static stress field: (a) Event density stress step-function δ(σ) (Eq. 5) of the Solid Seismicity Postulate (SSP) in comparison to the linear clock-change model; (b) Static stress σ versus distance r for different effective crack radii c and rupture stress drops $\Delta\sigma_0$ (Eq. 6); (c) Linear relationship between effective crack radius c and aftershock solid envelope radius r_* for different $\Delta\sigma_*/\Delta\sigma_0$ ratios (Eq. 7); (d) Relationship between mainshock magnitude M and effective crack radius c for different seismogenic widths w_0 (Eq. 8).

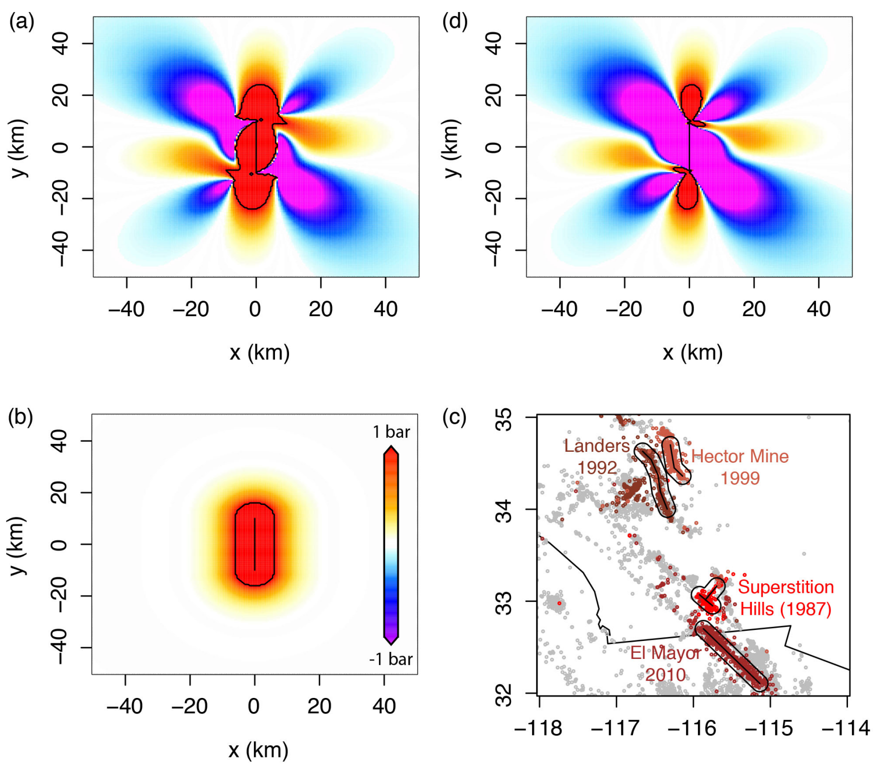

Figure 2. Possible static stress fields and inferred aftershock spatial distribution: (a) Right-lateral Coulomb stress field for optimally oriented faults, where the mainshock relieves all of the regional stresses σ_r = 10 bar, with $\Delta\sigma_0 \approx -Gs/L \approx$ - 10 bar (G = 3.3.10^5 bar the shear modulus, s = 0.6 m the slip, L = 20 km the fault length, and w = 10 km the fault width); (b) Radial static stress field computed from Eq. (6) with $\Delta\sigma_0$ = -10 bar and $c = \sqrt{(Lw)/\pi}$ for consistency with (a); (c) Aftershock distribution of the largest strike-slip events in the Southern California relocated catalog, identified here as all events occurring within one day of the mainshock; (d) Right-lateral Coulomb stress field for optimally oriented faults, where the mainshock relieves only a fraction of the regional stresses σ_r = 100 bar with $\Delta\sigma_0$ = -10 bar (same rupture as in (a)) – The black contour represents 1 bar in (a), (b) and (d), and a 10 km distance from rupture in

Nonlin. Processes Geophys. Discuss., https://doi.org/10.5194/npg-2017-38
Manuscript under review for journal Nonlin. Processes Geophys.
Discussion started: 18 July 2017

Nonlinear Processes in Geophysics
Discussions
Open Access

(c). Coulomb stress fields of (a) and (d) were computed using the Coulomb 3 software (Lin and Stein, 2004; Toda et al., 2005).

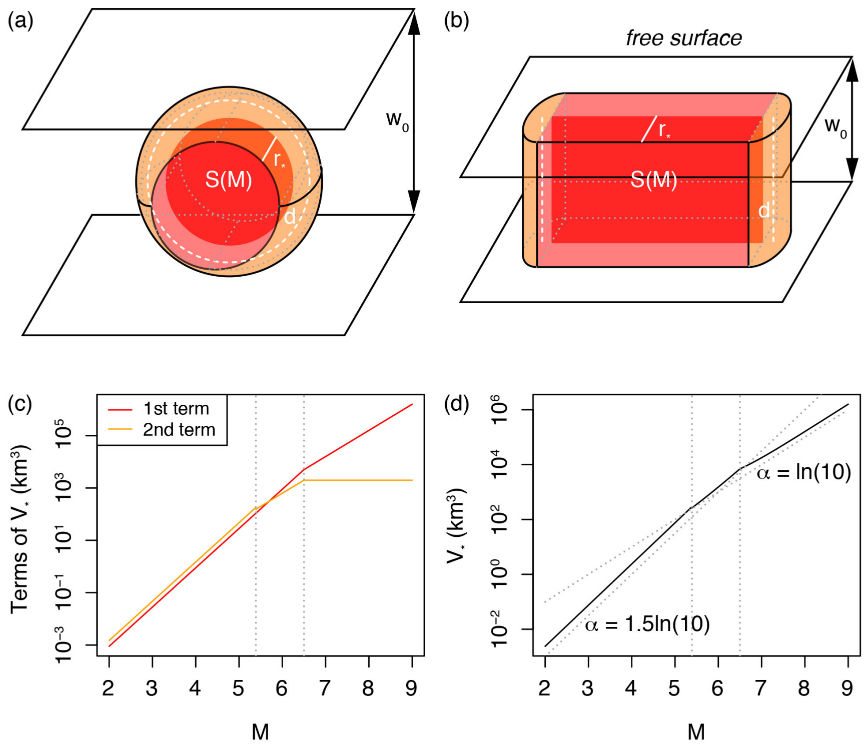

Figure 3. Geometric origin of the aftershock productivity law: (a) Sketch of the aftershock solid for a small mainshock rupture represented by a disk; (b) Sketch of the aftershock solid for a large mainshock rupture represented by a rectangle; (c) Relative role of the two terms of Eq. (9), here with w_0 = 10 km and $\frac{\Delta\sigma_*}{\Delta\sigma_0}$ = -0.1 (to first estimate c and r_* from Eqs. 8 and 7, respectively); (d) Aftershock productivity law (normalized by δ_+) predicted by Solid Seismicity (Eq. 11). This relationship is of the same form as the Utsu productivity law (Eq. 1) for large M (see text for an explanation of the lack

Nonlin. Processes Geophys. Discuss., https://doi.org/10.5194/npg-2017-38
Manuscript under review for journal Nonlin. Processes Geophys.
Discussion started: 18 July 2017

of break in scaling in Eq. 1 for small *M*). Dotted vertical lines represent *M* for $c(M) + r_*(M) = \frac{w_0}{2}$ and $S(M) = \pi w_0^2$, respectively.

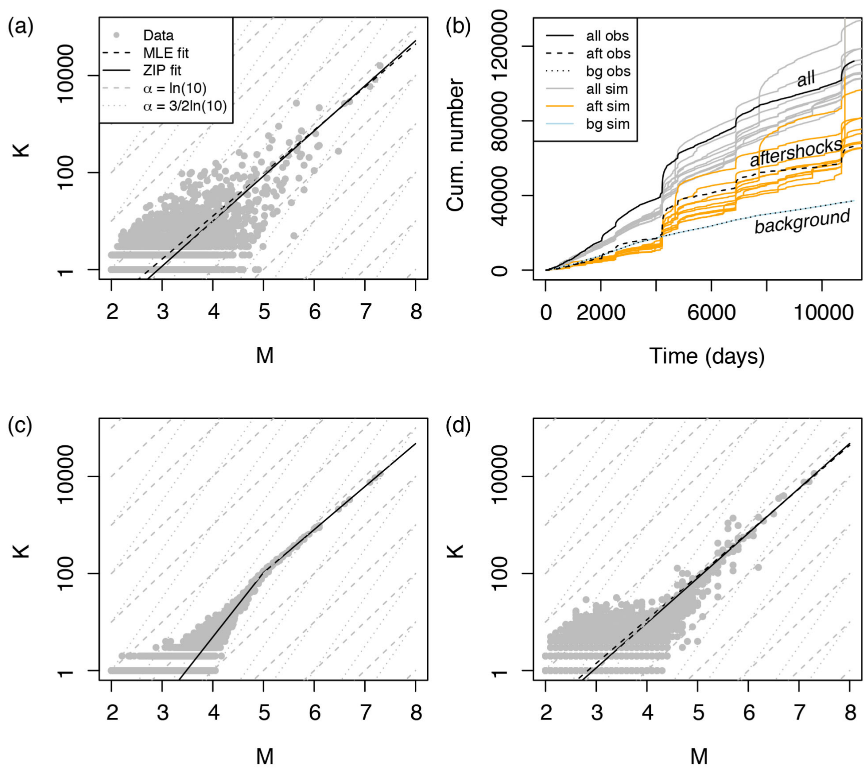

Figure 4. Aftershock productivity defined as the number of aftershocks $K(m_0 = 2)$ per mainshock of magnitude *M*: (a) Observed aftershock productivity in Southern California with aftershocks selected using the nearest-neighbor method; (b) Seismicity time series with distinction made between background events and aftershocks, observed ("obs", in black) and ETAS-simulated ("sim", colored); (c) True simulated aftershock productivity with kink, defined from Eq. (16); (d) Retrieved simulated aftershock productivity with aftershocks selected using the nearest-neighbor method - Data points in (a), (c) and (d) are represented by gray dots;

Nonlin. Processes Geophys. Discuss., https://doi.org/10.5194/npg-2017-38
Manuscript under review for journal Nonlin. Processes Geophys.
Discussion started: 18 July 2017

Nonlinear Processes in Geophysics
Open Access
Discussions

the model fits by Maximum Likelihood Estimation (MLE) method are represented by the dashed and solid black lines for the Poisson and Zero-Inflated Poisson distributions, respectively; dashed and dotted gray lines are visual guides to α = 3/2ln(10) and ln(10), respectively.